Semiclassical versus quantum behavior in fourth-order interference

Jeffrey H. Shapiro and Ke-Xun Sun*

Research Laboratory of Electronics, Massachusetts Institute of Technology, Cambridge, Massachusetts 02139-4307

Received July 1, 1993; revised manuscript received November 15, 1993

A theoretical construct is presented for fourth-order interference between the signal and the idler beams of a parametric downconverter. Previous quantum treatments of fourth-order interference have employed correlated single-photon wave packets. The introduced approach, however, relies on Gaussian-state field correlations, which were previously used to characterize quadrature-noise squeezing produced by an optical parametric amplifier and nonclassical twin-beam generation in an optical parametric oscillator. Three principal benefits accrue from the correlation-function formalism. First, the quantum theory of fourth-order interference is unified with that for the other nonclassical effects of $\chi^{(2)}$ interactions, i.e., squeezing and twin-beam production. Second, the semiclassical photodetection limit on Gaussian-state fourth-order interference is established; a purely quantum effect can be claimed at fringe visibilities substantially below the 50% level. Finally, both photon-coincidence counting (within the low-photon-flux regime) and intensity interferometry (in the high-photon-flux limit) are easily analyzed within a common framework.

1. INTRODUCTION

Parametric interactions in $\chi^{(2)}$ crystals have proved to be rich sources of nonclassical light-beam phenomena. When used in a resonant structure as a near-degenerate optical parametric amplifier (OPA), the $\chi^{(2)}$ interaction produces substantial quadrature-noise squeezing.[1] When such a structure is pumped above its oscillation threshold, the OPA becomes an optical parametric oscillator (OPO). In this regime the $\chi^{(2)}$ interaction yields nonclassical twin beams, i.e., strong signal and idler beams whose intensity correlation greatly exceeds classical bounds.[2] Finally, when used (without a resonator) as a parametric downconverter, the $\chi^{(2)}$ interaction becomes a source for nonclassically correlated, single-photon wave packets,[3] which in turn can be used to elicit nonclassical fourth-order interference effects.[4] All these phenomena originate from the same fundamental physics: in a $\chi^{(2)}$ material pumped by a strong beam at frequency ω_P and wave vector $\mathbf{k}_P$, a single pump photon is converted into a pair of photons—one signal (S) and one idler (I)—subject to the energy- and the momentum-conservation conditions, i.e., $\omega_S + \omega_I = \omega_P$ and $\mathbf{k}_S + \mathbf{k}_I = \mathbf{k}_P$, respectively.

Satisfactory quantum theories for all the preceding nonclassical light-beam phenomena are available, but a unified formalism encompassing them all has yet to appear. For example, both OPA squeezing and OPO twin beams are easily understood in terms of their field-quadrature spectra; see, e.g., Ref. 5 and Refs. 6 and 7, respectively. On the other hand, fourth-order interference is generally treated by means of correlated, single-photon wave packets; see, e.g., Refs. 8 and 9. More important, whereas the well-known semiclassical shot-noise limits of optical homodyne detection[10] and differenced direct detection[11] provide clear-cut boundaries beyond which purely quantum phenomena can be claimed in OPA and OPO experiments, the corresponding semiclassical bounds on fourth-order interference are, we believe, not widely appreciated. For example, it is often stated that the classical upper limit on fringe visibility in fourth-order interference is 50%,[8,12] implying that a purely quantum effect cannot be claimed at visibilities of less than 50%. This 50% ceiling is derived from a nonergodic classical-field model comprising monochromatic signal and idler beams whose frequencies are $\omega_S + \tilde{\omega}$ and $\omega_I - \tilde{\omega}$, respectively, where $\tilde{\omega}$ is a random variable with the appropriate probability distribution. In contrast, our theory for parametric downconverter fourth-order interference yields a much lower maximum fringe visibility in semiclassical photodetection. Also, our analytical framework provides the basis for directly refuting the assertion that the preceding nonergodic classical-field model yields 50%-visibility fringes.

In this paper we establish a formalism for analyzing fourth-order interference that parallels the approach taken in standard theories for squeezing. Aside from its merit in providing a unified framework for understanding all the nonclassical phenomena produced by $\chi^{(2)}$ interactions, this analysis will establish the fringe-visibility bound for the onset of nonclassical effects in Gaussian-state fourth-order interference. Furthermore, our fourth-order interference treatment extends into the high-photon-flux regime, such as might be approached in a resonant-structure OPA. Here we develop results for intensity interferometry measurements, a hitherto unexplored regime, as opposed to the more usual photon-coincidence measurements. It will turn out that purely quantum effects are harder to discern in high-photon-flux intensity interferometry. For brevity we focus our attention on analyzing two recent fourth-order interference experiments: the dispersion-cancellation experiments of Steinberg *et al.*[13,14] and the Mach–Zehnder measurements of Shih *et al.*[15] Together these configurations span both degenerate and nondegenerate operation, and our analyses of them amply demonstrate the great convenience of the field-correlation formalism. We shall see

0740-3224/94/061130-12$06.00 ©1994 Optical Society of America

that the results of these experiments arise from the linear filtering of the quantum-field operators as manifest through photon-coincidence-counting interference. As our treatment makes clear, this linear filtering mimics classical propagation through each experiment's optical setup, whereas the high-visibility photon-coincidence fringes are due to the parametric downconverter's entangled joint signal–idler state. Dispersion cancellation, for example, is really a classical effect. Its observation by photon-coincidence counting, however, requires a nonclassical light source.

The starting point for all our work is a pair of models, one quantum and one classical, for the signal and the idler fields produced by parametric downconversion. These field models, in turn, feed into the standard descriptions of quantum and semiclassical photodetection, leading almost immediately to the desired fourth-order interference results.

2. FIELD AND PHOTODETECTION MODELS

Consider an idealized parametric downconverter that is driven by a stable, continuous-wave (cw) pump at frequency ω_P, producing cw signal and idler beams at center frequencies ω_S and $\omega_I = \omega_P - \omega_S$, respectively. Suppressing, for simplicity, the spatial and polarization characteristics of these fields, relying on a photon-units formulation (see Ref. 16), and assuming perfect signal–idler correlation, we can employ the following statistical models.

A. Quantum Fields and Quantum Photodetection

Let $\hat{E}_S(t)$ and $\hat{E}_I(t)$ be the positive-frequency signal and idler field operators, respectively, at the output of the parametric downconverter.[17] These operators commute with each other (and with each other's adjoint) and individually satisfy the delta-function commutator rule

$$[\hat{E}_j(t), \hat{E}_j^{\dagger}(u)] = \delta(t-u), \qquad \text{for } j = S, I. \tag{1}$$

The joint density operator for the signal and the idler is a zero-mean-field Gaussian state,[18] which is completely characterized by the following normally ordered and phase-sensitive correlations for $j = S, I$ and $k = S, I$:

$$\langle \hat{E}_j^{\dagger}(t+\tau)\hat{E}_k(t)\rangle = \delta_{jk}\exp(i\omega_j\tau)\int \frac{d\omega}{2\pi}\,\mathcal{P}(\omega)\exp(i\omega\tau), \tag{2}$$

$$\begin{aligned}\langle \hat{E}_j(t+\tau)\hat{E}_k(t)\rangle = (1-\delta_{jk})&\exp[-i(\omega_P t + \omega_j\tau)] \\ &\times \int \frac{d\omega}{2\pi}\{\mathcal{P}(\omega)[\mathcal{P}(\omega)+1]\}^{1/2} \\ &\times \exp(-i\omega\tau),\end{aligned} \tag{3}$$

where δ_{jk} is the Kronecker delta function and $\mathcal{P}(\omega) \geq 0$ is the common signal and idler spectrum.

A useful, intuitive picture for the preceding downconverter model is as follows. Let $\hat{E}_S^{\mathrm{IN}}(t)$ and $\hat{E}_I^{\mathrm{IN}}(t)$ be the positive-frequency signal and idler field operators, respectively, at the input to the downconverter. These operators share the free-field commutator properties exhibited above for the downconverter's output fields. Moreover, for the operating conditions of interest to us, these input fields are both unexcited, i.e., they are in their vacuum states. Introducing input and output frequency-domain field operators

$$\hat{\mathcal{E}}_j^{\mathrm{IN}}(\omega) \equiv \int dt\,\hat{E}_j^{\mathrm{IN}}(t)\exp(i\omega t) \qquad \text{for } j = S, I, \tag{4}$$

$$\hat{\mathcal{E}}_j(\omega) \equiv \int dt\,\hat{E}_j(t)\exp(i\omega t) \qquad \text{for } j = S, I, \tag{5}$$

we can show that the joint state posited above for the parametric downconverter's output beams is generated by the well-known, frequency-domain Bogoliubov transformations for $\chi^{(2)}$ coupled-mode interactions, namely,

$$\begin{aligned}\hat{\mathcal{E}}_S(\omega_S+\omega) = &[\mathcal{P}(\omega)+1]^{1/2}\hat{\mathcal{E}}_S^{\mathrm{IN}}(\omega_S+\omega) \\ &+ [\mathcal{P}(\omega)]^{1/2}\hat{\mathcal{E}}_I^{\mathrm{IN}\dagger}(\omega_I-\omega),\end{aligned} \tag{6}$$

$$\begin{aligned}\hat{\mathcal{E}}_I(\omega_I-\omega) = &[\mathcal{P}(\omega)+1]^{1/2}\hat{\mathcal{E}}_I^{\mathrm{IN}}(\omega_I-\omega) \\ &+ [\mathcal{P}(\omega)]^{1/2}\hat{\mathcal{E}}_S^{\mathrm{IN}\dagger}(\omega_S+\omega).\end{aligned} \tag{7}$$

It has long been known that Bogoliubov transformations produce squeezing.[19] Furthermore, Eqs. (6) and (7) preserve the photon-number difference, that is,

$$\begin{aligned}&\hat{\mathcal{E}}_S^{\dagger}(\omega_S+\omega)\hat{\mathcal{E}}_S(\omega_S+\omega) - \hat{\mathcal{E}}_I^{\dagger}(\omega_I-\omega)\hat{\mathcal{E}}_I(\omega_I-\omega) \\ &\quad = \hat{\mathcal{E}}_S^{\mathrm{IN}\dagger}(\omega_S+\omega)\hat{\mathcal{E}}_S^{\mathrm{IN}}(\omega_S+\omega) \\ &\qquad - \hat{\mathcal{E}}_I^{\mathrm{IN}\dagger}(\omega_I-\omega)\hat{\mathcal{E}}_I^{\mathrm{IN}}(\omega_I-\omega) \qquad \text{for all } \omega.\end{aligned} \tag{8}$$

Because the right-hand side of Eq. (8) is essentially the photon-number difference between two vacuum-state modes, we see that Eqs. (6) and (7) imply a photon-twins behavior. Specifically, for each output signal-beam photon at frequency $\omega_S + \omega$, there must be a corresponding output idler-beam photon at frequency $\omega_I - \omega$.

In using Eqs. (2) and (3), we assume that $\mathcal{P}(\omega)$ is an even function of ω. This restriction entails no significant loss of generality for our purposes and represents a typical condition for $\chi^{(2)}$ interactions; cf. Eq. (9). Note that we have omitted a possible frequency-dependent phase factor within the integral in Eq. (3); inclusion of such a factor is analogous to the dispersion term that is seen below in our analysis of the dispersion-cancellation experiment. For relevance to other studies of fourth-order interference in parametric downconversion and for calculational convenience it is of value to assume that $\mathcal{P}(\omega)$ is given by

$$\mathcal{P}(\omega) = (\sqrt{2\pi}\,P/\Delta\omega)\exp(-\omega^2/2\Delta\omega^2), \tag{9}$$

which implies that

$$\begin{aligned}\langle \hat{E}_S^{\dagger}(t+\tau)\hat{E}_S(t)\rangle\exp(-i\omega_S\tau) &= \langle \hat{E}_I^{\dagger}(t+\tau)\hat{E}_I(t)\rangle \\ &\quad \times \exp(-i\omega_I\tau) \\ &= P\exp(-\tau^2\Delta\omega^2/2).\end{aligned} \tag{10}$$

Thus both the signal and the idler beams have Gaussian spectra, with P photons/s on average, $\Delta\omega$-s^{-1} bandwidths, and transform-limited $\Delta\omega^{-1}$-s coherence times.

The phase-sensitive correlation that is associated with the Gaussian spectrum from Eq. (9) cannot be expressed in closed form. Nevertheless, two physically important

special cases can be discerned, one of which leads to a useful closed-form approximation for Eq. (3). First, there is the low-photon-flux regime, wherein $P/\Delta\omega \ll 1$ prevails. Here the average number of signal and idler photons per coherence time is much smaller than 1, and we can use $\mathcal{P}(\omega) \ll 1$ to obtain

$$\begin{aligned}\langle \hat{E}_S(t+\tau)\hat{E}_I(t)\rangle &\exp(i\omega_S\tau) \\ &= \langle \hat{E}_I(t+\tau)\hat{E}_S(t)\rangle \exp(i\omega_I\tau) \\ &\approx (2/\pi)^{1/4}\sqrt{P\Delta\omega}\,\exp(-i\omega_P t - \tau^2\Delta\omega^2). \quad (11)\end{aligned}$$

Second, the high-photon-flux limit, wherein $P/\Delta\omega \gg 1$ holds, is also interesting. Here there are large numbers of signal and idler photons, on average, per coherence time, and we are tempted to use $\{\mathcal{P}(\omega)[\mathcal{P}(\omega)+1]\}^{1/2} \approx \mathcal{P}(\omega)$, which applies over the dominant low-frequency spectral region, to argue that

$$\begin{aligned}\langle \hat{E}_S(t+\tau)\hat{E}_I(t)\rangle \exp(i\omega_S\tau) &= \langle \hat{E}_I(t+\tau)\hat{E}_S(t)\rangle \exp(i\omega_I\tau) \\ &\approx P\,\exp(-i\omega_P t - \tau^2\Delta\omega^2/2). \quad (12)\end{aligned}$$

Unfortunately, as we explain in Subsection 2.B, this is a temptation that must be resisted—it throws away the nonclassical behavior of the joint signal–idler state.

To complete the laying of our quantum foundation, we need only append the standard photon-flux model for quantum photodetection,[10,16] which states that a unity-quantum-efficiency detector illuminated by a delta-function commutator photon-units field operator $\hat{E}(t)$ produces a classical stochastic photocurrent $i(t)$, whose classical statistics are identical to those of the quantum operator $\hat{i}(t) \equiv q\hat{E}^\dagger(t)\hat{E}(t)$, where q is the charge released per photon absorption.[20] Thus, for example, if we illuminate one such detector with the signal beam and another such detector with the idler beam, then we obtain two classical photocurrents, $i_S(t)$ and $i_I(t)$, which are equivalent to the quantum operators $\hat{i}_S(t) \equiv q\hat{E}_S{}^\dagger(t)\hat{E}_S(t)$ and $\hat{i}_I(t) \equiv q\hat{E}_I{}^\dagger(t)\hat{E}_I(t)$, respectively. These operator representations are used below to demonstrate that our zero-mean-field joint Gaussian signal–idler state, with correlations specified by Eqs. (2) and (3), embodies perfect signal–idler photon correlation, just as is seen in the linearized Gaussian-state field-correlation treatment of OPO photon-twins beams.[6,7] If, on the other hand, we combine a 50/50 mixture of the signal and the idler with a strong local-oscillator beam—with P_{LO} photons/s, frequency $\omega_P/2$, and phase θ—in a unity-quantum-efficiency balanced homodyne receiver, quantum photodetection predicts that we will obtain a classical stochastic photocurrent $i_\theta(t)$ equivalent to the quantum operator measurement of

$$\hat{i}_\theta(t) \equiv q\,\mathrm{Re}\{\sqrt{2P_{\mathrm{LO}}}\,\exp[i(\omega_P t/2 - \theta)][\hat{E}_S(t) + \hat{E}_I(t)]\}. \quad (13)$$

This equation is used below to elicit the standard OPA squeezing results from our zero-mean-field joint Gaussian signal–idler state model; cf. Ref. 5.

B. Classical Fields and Semiclassical Photodetection

The classical-field model that most closely mimics the preceding quantum model corresponds to classically random, positive-frequency, photon-units signal and idler fields $E_S(t)$ and $E_I(t)$. These fields comprise a pair of zero-mean, complex-valued, jointly Gaussian random processes, which are completely characterized by the following normally ordered and phase-sensitive correlations for $j = S,I$, and $k = S,I$:

$$\langle E_j{}^*(t+\tau)E_k(t)\rangle = \delta_{jk}\exp(-i\omega_j\tau)\int \frac{d\omega}{2\pi}\,\mathcal{P}(\omega)\exp(i\omega\tau), \quad (14)$$

$$\begin{aligned}\langle E_j(t+\tau)E_k(t)\rangle &= (1-\delta_{jk})\exp[-i(\omega_P t + \omega_j\tau)] \\ &\quad \times \int \frac{d\omega}{2\pi}\,\mathcal{P}(\omega)\exp(-i\omega\tau), \quad (15)\end{aligned}$$

when the angle brackets now denote a classical ensemble average instead of a quantum average. Once again we assume that $\mathcal{P}(\omega)$ is an even function of ω, and we note that a frequency-dependent phase factor could be included inside the integral in the phase-sensitive correlation. Also, as was stated for the quantum model, we employ the Gaussian spectrum, Eq. (9), in the calculations built on this classical construct:

$$\begin{aligned}\langle E_S{}^*(t+\tau)E_S(t)\rangle &\exp(-i\omega_S\tau) \\ &= \langle E_I{}^*(t+\tau)E_I(t)\rangle \exp(-i\omega_I\tau) \\ &= P\,\exp(-\tau^2\Delta\omega^2/2), \quad (16) \\ \langle E_S(t+\tau)E_I(t)\rangle \exp(i\omega_S\tau) &= \langle E_I(t+\tau)E_S(t)\rangle \exp(i\omega_I\tau) \\ &= P\,\exp(-i\omega_P t - \tau^2\Delta\omega^2/2), \quad (17)\end{aligned}$$

are the Gaussian-spectrum correlations for the classical model. Note that Eq. (17) is exact, and it coincides with the specious high-photon-flux quantum approximation, relation (12), presented in Subsection 2.A. The problem with relation (12) can now be stated explicitly: it makes the quantum photodetection model for parametric downconversion exactly equal to the semiclassical photodetection model for the downconverter. This implied equivalence will be demonstrated below, following our review of semiclassical photodetection.

In semiclassical photodetection the illuminating field is considered classical, and random emission of charge quanta introduces shot noise into the process of optical-to-electrical conversion. For our classical, photon-units field model this implies that ideal unity-quantum-efficiency direct detection of a classical field $E(t)$ produces a photocurrent $i(t)$ that is an inhomogeneous conditional Poisson impulse train of conditional rate $|E(t)|^2$; see Ref. 16. More-explicit results are obtained if we limit our interest to the first and second moments of the photocurrent. Within this more restricted domain we can say that

$$i(t) = q|E(t)|^2 + i_n(t), \quad (18)$$

where $i_n(t)$, the shot noise, has zero mean and the covariance function

$$\langle i_n(t)i_n(u)\rangle = q^2\langle |E(t)|^2\rangle\delta(t-u) \quad (19)$$

and is uncorrelated with the classical photon-units intensity $|E(t)|^2$ illuminating the detector. At constant average intensity the covariance is stationary, giving rise to the well-known shot-noise spectrum,

$$S_{\text{shot}}(\omega) \equiv \int \mathrm{d}\tau \langle i_n(t+\tau) i_n(t) \rangle \exp(-i\omega\tau) = q^2 \langle |E|^2 \rangle . \tag{20}$$

Equations (18)–(20) can be applied to direct detection of either the signal or the idler beams of our classical field model. Moreover, because the shot noise of physically different detectors is statistically independent (in open-loop semiclassical photodetection[21]), these equations can also be combined to handle differenced direct detection of the signal and the idler beams, as is done below. Finally, if we combine a 50/50 mixture of the signal and the idler beams with a strong local oscillator in a unity-quantum-efficiency balanced homodyne receiver, semiclassical photodetection theory predicts that we will obtain a photocurrent $i_\theta(t)$ that obeys

$$i_\theta(t) = q \, \mathrm{Re}\{\sqrt{2P_{\text{LO}}} \exp[i(\omega_P t/2 - \theta)][E_S(t) + E_I(t)]\} + i_{\text{LO}}(t) . \tag{21}$$

Here, $i_{\text{LO}}(t)$ is the local-oscillator shot noise, that is, a zero-mean, stationary, white Gaussian noise with spectrum $q^2 P_{\text{LO}}$.

Starting in the next subsection, and continuing throughout the remainder of the paper, we compare the predictions of the preceding quantum and semiclassical models. Before we get to the specifics, however, one general point is germane. It turns out that any photodetection measurement that distinguishes between these two models must invoke the joint statistics of the signal and the idler beams. In particular, because the quantum model assumes that the signal and the idler beams are in a zero-mean jointly Gaussian state, they must individually be in zero-mean Gaussian states.[19] Moreover, because the signal-only and the idler-only density operators have, by means of Eq. (3), phase-insensitive noises, they are both classically random mixtures of coherent states. Thus semiclassical photodetection can be employed for signal-only or idler-only measurements, with Eq. (2) supplying the necessary classical-field normally ordered correlation functions. Finally, because Eqs. (2) and (14) coincide, our quantum and semiclassical models predict exactly the same photodetection statistics for any such signal-only or idler-only measurements.

The distinction between our two models of parametric downconversion lies in the nonclassical entanglement between the signal and the idler beams, that is, the +1 within the square root in Eq. (3) that is absent from Eq. (15). This is why we cannot use relation (12) in the high-photon-flux quantum regime. In particular, because relation (12) equals the classical phase-sensitive correlation function [Eq. (17)], the zero-mean-field jointly Gaussian signal–idler state whose normally ordered and phase-sensitive correlation functions are given by Eq. (10) and relation (12) is classical. Hence the quantum-photodetection statistics for joint signal–idler measurements for this state are identical to the corresponding semiclassical-photodetection predictions for such measurements. The two models are then entirely indistinguishable.

C. Quantum Signatures In Squeezing and Photon Twins

Having focused attention on the +1 in Eq. (3), it is time to review two of the purely quantum effects that it creates: squeezing and photon twins. These effects were foreseen in our comments regarding the Bogoliubov transformations, Eqs. (6) and (7). Our present purpose is to derive them from the full time-domain statistics of the downconverter's output beams.

Let us begin with the homodyne observation of quadrature-noise squeezing for a degenerate parametric downconverter, i.e., for the case $\omega_S = \omega_I = \omega_P/2$. Under both our quantum and semiclassical models the homodyne photocurrent $i_\theta(t)$ is then a zero-mean, stationary, Gaussian random process with a phase-sensitive, i.e., a θ-dependent noise spectrum. For the quantum model, Eq. (13) and Eqs. (1)–(3) yield

$$\begin{aligned} S_\theta(\omega) &\equiv \int \mathrm{d}\tau \langle i_\theta(t+\tau) i_\theta(t) \rangle \exp(-i\omega\tau) \\ &= q^2 P_{\text{LO}} |[1 + \mathcal{P}(\omega)]^{1/2} + \exp(-i2\theta)[\mathcal{P}(\omega)]^{1/2}|^2 \end{aligned} \tag{22}$$

for this noise spectrum, whereas Eq. (21), with Eqs. (14) and (15), gives the corresponding semiclassical result,

$$S_\theta(\omega) = q^2 P_{\text{LO}}[1 + \mathcal{P}(\omega)|1 + \exp(-i2\theta)|^2] . \tag{23}$$

When $\theta = \pi/2$, both spectra are minimized at all frequencies:

$$S_{\min}(\omega) = \begin{cases} q^2 P_{\text{LO}}\{[1 + \mathcal{P}(\omega)]^{1/2} - [\mathcal{P}(\omega)]^{1/2}\}^2 & \text{quantum theory} \\ q^2 P_{\text{LO}} & \text{semiclassical theory} \end{cases} . \tag{24}$$

Thus the semiclassical noise level always equals or exceeds the shot-noise limit, whereas the quantum theory can have noise lower than the shot-noise limit.[22] The latter statement follows readily from

$$(\sqrt{1+x} - \sqrt{x})^2 = 1/(\sqrt{1+x} + \sqrt{x})^2 < 1 \qquad \text{for } x > 0 , \tag{25}$$

from which it can also be seen that to have a strongly nonclassical effect requires that $\mathcal{P}(\omega) \sim 1$ in Eq. (24). This is why cavity-resonance enhancement is used in cw OPA's to show appreciable quadrature-noise squeezing: single-pass cw parametric downconversion almost always leads to $\mathcal{P}(\omega) \ll 1$.

Now let us turn to the photon-twin aspect of our quantum and semiclassical parametric downconversion models. Note that, unlike the previous treatment of quadrature-noise squeezing and the linearized analysis of OPO twin beams, in which the signal and the idler beams' mean fields act as local oscillators,[6,7] analyzing downconverter photon twins will require fourth-order field moments. As such, it offers a useful entrée to our main task, i.e., understanding fourth-order interference. Consider differenced direct detection of the signal and the idler beams of a nondegenerate parametric downconverter

leading to a different photocurrent $\Delta i(t) \equiv i_S(t) - i_I(t)$. In both our quantum and semiclassical models $\Delta i(t)$ is a zero-mean, stationary random process. We are interested in

$$\Delta N_T \equiv q^{-1} \int_{-T/2}^{T/2} dt \Delta i(t), \tag{26}$$

which is the signal-minus-idler photocount difference over the time interval $-T/2 < t \leq T/2$. Both of our photodetection models imply that ΔN_T is a zero-mean random variable for all T. To evaluate the variance of ΔN_T, we need to find the spectrum of $\Delta i(t)$, namely,

$$S_{\Delta i}(\omega) \equiv \int d\tau \langle \Delta i(t+\tau) \Delta i(t) \rangle \exp(-i\omega\tau), \tag{27}$$

as predicted by our two models.

For the quantum model we rely on the operator photocurrent representations and their associated commutator brackets to obtain

$$\begin{aligned}\langle \Delta i(t+\tau) \Delta i(t) \rangle = q^2 \{ & \delta(\tau) [\langle \hat{E}_S^\dagger(t) \hat{E}_S(t) \rangle + \langle \hat{E}_I^\dagger(t) \hat{E}_I(t) \rangle] \\ & + \langle \hat{E}_S^\dagger(t+\tau) \hat{E}_S^\dagger(t) \hat{E}_S(t+\tau) \hat{E}_S(t) \rangle \\ & + \langle \hat{E}_I^\dagger(t+\tau) \hat{E}_I^\dagger(t) \hat{E}_I(t+\tau) \hat{E}_I(t) \rangle \\ & - \langle \hat{E}_S^\dagger(t+\tau) \hat{E}_I^\dagger(t) \hat{E}_S(t+\tau) \hat{E}_I(t) \rangle \\ & - \langle \hat{E}_I^\dagger(t+\tau) \hat{E}_S^\dagger(t) \hat{E}_I(t+\tau) \hat{E}_S(t) \rangle \}. \end{aligned} \tag{28}$$

With the quantum form of the Gaussian moment-factoring theorem[23,24] these fourth moments can be reduced to sums of products of second moments, which are available from Eqs. (2) and (3), leading to

$$\begin{aligned}\langle \Delta i(t+\tau) \Delta i(t) \rangle = q^2 \{ & \delta(\tau) [\langle \hat{E}_S^\dagger(t) \hat{E}_S(t) \rangle + \langle \hat{E}_I^\dagger(t) \hat{E}_I(t) \rangle] \\ & + \langle \hat{E}_S^\dagger(t+\tau) \hat{E}_S(t) \rangle \langle \hat{E}_S^\dagger(t) \hat{E}_S(t+\tau) \rangle \\ & + \langle \hat{E}_I^\dagger(t+\tau) \hat{E}_I(t) \rangle \langle \hat{E}_I^\dagger(t) \hat{E}_I(t+\tau) \rangle \\ & - \langle \hat{E}_S^\dagger(t+\tau) \hat{E}_I^\dagger(t) \rangle \langle \hat{E}_S(t+\tau) \hat{E}_I(t) \rangle \\ & - \langle \hat{E}_I^\dagger(t+\tau) \hat{E}_S^\dagger(t) \rangle \langle \hat{E}_I(t+\tau) \hat{E}_S(t) \rangle \}. \end{aligned} \tag{29}$$

A Fourier transformation now yields[25]

$$\begin{aligned} S_{\Delta i}(\omega) = 2q^2 \int \frac{d\omega'}{2\pi} \{ & \mathcal{P}(\omega') + \mathcal{P}(\omega') \mathcal{P}(\omega' - \omega) \\ & - [\mathcal{P}(\omega') [\mathcal{P}(\omega') + 1] \mathcal{P}(\omega' - \omega) [\mathcal{P}(\omega' - \omega) + 1]]^{1/2} \}. \end{aligned} \tag{30}$$

At zero frequency the difference photocurrent's spectrum vanishes, $S_{\Delta i}(0) = 0$, whereas at high frequencies it approaches the semiclassical shot-noise formula,

$$\lim_{\omega \to \infty} S_{\Delta i}(\omega) = 2q^2 \int \frac{d\omega'}{2\pi} \mathcal{P}(\omega'). \tag{31}$$

For the Gaussian spectrum, from Eq. (9), the transition between these two regimes occurs at $\omega \approx \Delta\omega$. We make the significance of these results clear after we develop the semiclassical formula for $S_{\Delta i}(\omega)$.

The semiclassical spectrum of $\Delta i(t)$ is rather different from that seen in Eq. (30). In this case we have that

$$\Delta i(t) = q[|E_S(t)|^2 - |E_I(t)|^2] + \Delta i_n(t), \tag{32}$$

where $\Delta i_n(t)$ is the difference of the statistically independent shot noises from the two photodetectors. This noise current is therefore a zero-mean, stationary random process whose spectrum, found by adding the shot-noise spectra of the signal and the idler photocurrents [cf. Eq. (20)], is $q^2[\langle |E_S(t)|^2 \rangle + \langle |E_I(t)|^2 \rangle]$. To find the spectrum of $\Delta i(t)$, we must add to this shot-noise term the contribution from the photon-flux difference, $q[|E_S(t)|^2 - |E_I(t)|^2]$. This is easily done in parallel to the development of Eq. (28). We find that the semiclassical model gives

$$\begin{aligned}\langle \Delta i(t+\tau) \Delta i(t) \rangle = q^2 \{ & \delta(\tau) [\langle |E_S(t)|^2 \rangle + \langle |E_I(t)|^2 \rangle] \\ & + \langle E_S^*(t+\tau) E_S^*(t) E_S(t+\tau) E_S(t) \rangle \\ & + \langle E_I^*(t+\tau) E_I^*(t) E_I(t+\tau) E_I(t) \rangle \\ & - \langle E_S^*(t+\tau) E_I^*(t) E_S(t+\tau) E_I(t) \rangle \\ & - \langle E_I^*(t+\tau) E_S^*(t) E_I(t+\tau) E_S(t) \rangle \}. \end{aligned} \tag{33}$$

Employing the classical Gaussian moment-factoring theorem[24] and the correlation functions from Eqs. (14) and (15) then provides

$$\langle \Delta i(t+\tau) \Delta i(t) \rangle = q^2 \delta(\tau) [\langle |E_S(t)|^2 \rangle + \langle |E_I(t)|^2 \rangle], \tag{34}$$

whence, on Fourier transformation, we find that the semiclassical difference photocurrent is shot-noise limited[25]:

$$S_{\Delta i}(\omega) = 2q^2 \int \frac{d\omega'}{2\pi} \mathcal{P}(\omega') = 2q^2 P, \tag{35}$$

at all frequencies, where the integral has been evaluated with the Gaussian spectrum from Eq. (9) assumed.

Comparing Eqs. (30) and (35) reveals that the nonclassical signal–idler entanglement is evident at frequencies below the emission bandwidth $\Delta\omega$. In particular, the per-unit-time variance of the photocount difference satisfies

$$\langle \Delta N_T^2 \rangle / T = \int \frac{d\omega}{2\pi} T \left[\frac{\sin(\omega T/2)}{\omega T/2} \right]^2 S_{\Delta i}(\omega). \tag{36}$$

Using Eqs. (30) and (35), plus the Gaussian spectrum from Eq. (9), then shows us that

$$\langle \Delta N_T^2 \rangle / T = 2P \qquad \text{for all } T \tag{37}$$

in the semiclassical theory, whereas the quantum theory predicts that

$$\langle \Delta N_T^2 \rangle / T \to \begin{cases} 2P & \text{as } \Delta\omega T \to 0 \\ 0 & \text{as } \Delta\omega T \to \infty \end{cases}. \tag{38}$$

Thus the semiclassical per-unit-time photocount variance is always shot-noise limited, but the quantum expression drops substantially below this limit, with increasing T, once $\Delta\omega T \gg 1$. Physically each signal–idler photon pair produced by the parametric downconversion process has a time uncertainty of the order of $\Delta\omega^{-1}$ between its two component members. That is why we must integrate over many of these coherence times if we are to sense the nonclassical entanglement of the signal and the idler beams.

3. FOURTH-ORDER INTERFERENCE

We are now ready for the analysis of two fourth-order interference experiments: the dispersion-cancellation measurements of Steinberg *et al.*[13,14] and the nondegenerate Mach–Zehnder measurements of Shih *et al.*[15] We begin with the experiment of Steinberg *et al.* Their arrangement is a modification of the configuration used by Hong *et al.*[26] to exhibit the time duration of the parametric downconverter's entangled single-photon wave packets. Furthermore, the dispersion-cancellation experiment uses a degenerate downconverter, so its analysis is somewhat simpler than that for the interferometer of Shih *et al.*, which employs nondegenerate signal and idler beams.

A. Dispersion-Cancellation Experiment

Figure 1 shows a schematic for the experiment of Steinberg *et al.*[13,14] Signal and idler beams—modeled as in Section 2 for use in quantum and semiclassical photodetection—are produced by an ideal degenerate parametric downconverter. The signal beam is subjected to propagation through a lossless, linear, dispersive element and then combined with the idler beam on the surface of a movable 50/50 beam splitter. The output beams from this beam splitter are measured by two unity-quantum-efficiency photodetectors, and average single-detector-count rates and a coincidence-count rate are determined by time averaging. These count rates are accumulated as functions of a variable path-length difference produced by beam-splitter motion.

We can quantify the Fig. 1 setup as follows. In the quantum theory the signal and the idler beams are given by the field operators $\hat{E}_S(t)$ and $\hat{E}_I(t)$, respectively; the joint state of the beams is as specified in Subsection 2.A. The output of the dispersive element is then a dispersively filtered signal beam,

$$\hat{E}_{\mathrm{SD}}(t) \equiv \int \mathrm{d}\tau \hat{E}_S(\tau) h(t-\tau), \tag{39}$$

where

$$h(t) \equiv \exp(-i\omega_S t) \int \frac{\mathrm{d}\omega}{2\pi} H(\omega) \exp(i\omega t) \tag{40}$$

is the impulse response of a lossless, dispersive filter whose frequency response

$$H(\omega) \equiv \exp(i\omega^2 \ddot{\phi}/2) \tag{41}$$

has the standard Taylor-expansion form with dispersion constant $\ddot{\phi}$. This filter will spread a transform-limited Gaussian pulse of bandwidth $\Delta\omega$ s^{-1} and duration $\Delta\omega^{-1}$ s into a $\Delta\omega$-bandwidth chirped-Gaussian pulse of duration

$$\Delta t = (1 + \ddot{\phi}^2 \Delta\omega^4)^{1/2} / \Delta\omega . \tag{42}$$

Note that we have suppressed the group-delay term in $H(\omega)$ by assuming that the beam splitter's zero-delay point has been chosen to compensate for this effect.

The lossless, linear filtering of $\hat{E}_S(t)$ preserves the delta-function commutator

$$[\hat{E}_{\mathrm{SD}}(t), \hat{E}_{\mathrm{SD}}{}^{\dagger}(u)] = \delta(t-u), \tag{43}$$

as it must if Eq. (39) is to characterize a photon-units field operator correctly. More important, this filter does not disturb the jointly Gaussian state of the signal–idler pair, i.e., $\hat{E}_{\mathrm{SD}}(t)$ and $\hat{E}_I(t)$ are still in a zero-mean-field jointly Gaussian state.[27,28] From standard moment-propagation formulas for linear filters, the jointly Gaussian state of $\hat{E}_{\mathrm{SD}}(t)$ and $\hat{E}_I(t)$ is then completely characterized by the following correlation functions [cf. Eqs. (2) and (3)]:

$$\langle \hat{E}_j{}^{\dagger}(t+\tau) \hat{E}_k(t) \rangle = \delta_{jk} \exp(i\omega_j \tau) \int \frac{\mathrm{d}\omega}{2\pi} \mathcal{P}(\omega) \exp(i\omega\tau), \tag{44}$$

$$\begin{aligned} \langle \hat{E}_j(t+\tau) \hat{E}_k(t) \rangle = (1-\delta_{jk}) &\exp[-i(\omega_P t + \omega_j \tau)] \\ &\times \int \frac{\mathrm{d}\omega}{2\pi} \{\mathcal{P}(\omega)[\mathcal{P}(\omega)+1]\}^{1/2} \\ &\times H(\omega) \exp(-i\omega\tau), \end{aligned} \tag{45}$$

which apply for $j = \mathrm{SD}, I$ and $k = \mathrm{SD}, I$, with $\omega_{\mathrm{SD}} \equiv \omega_S$. For the sake of brevity, we limit our treatment of the dispersion-cancellation experiment to the Gaussian spectrum from Eq. (9) in the low-photon-flux regime; see relation (11). The nonzero correlations from Eqs. (44) and (45) then become

$$\begin{aligned} \langle \hat{E}_{\mathrm{SD}}{}^{\dagger}(t+\tau) \hat{E}_{\mathrm{SD}}(t) \rangle &= \langle \hat{E}_I{}^{\dagger}(t+\tau) \hat{E}_I(t) \rangle \\ &= P \exp(i\omega_P \tau/2 - \tau^2 \Delta\omega^2/2), \end{aligned} \tag{46}$$

$$\begin{aligned} \langle \hat{E}_{\mathrm{SD}}(t+\tau) \hat{E}_I(t) \rangle &= \langle \hat{E}_I(t+\tau) \hat{E}_{\mathrm{SD}}(t) \rangle \\ &\approx \left(\frac{2}{\pi}\right)^{1/4} \left(\frac{P\Delta\omega}{1 - 2i\ddot{\phi}\Delta\omega^2}\right)^{1/2} \\ &\times \exp\left[-i\omega_P(t+\tau/2) - \frac{\tau^2\Delta\omega^2}{1-2i\ddot{\phi}\Delta\omega^2}\right], \end{aligned} \tag{47}$$

where we have used the degeneracy condition $\omega_S = \omega_I = \omega_P/2$.

The rest of the analytical setup is straightforward. The beam splitter produces the field operators

$$\hat{E}_1(t) \equiv [\hat{E}_{\mathrm{SD}}(t - T/2) + \hat{E}_I(t)]/\sqrt{2}, \tag{48}$$

$$\hat{E}_2(t) \equiv [\hat{E}_{\mathrm{SD}}(t) - \hat{E}_I(t + T/2)]/\sqrt{2} \tag{49}$$

that illuminate unity-quantum-efficiency photodetectors 1 and 2, respectively, where T is the beam splitter's variable delay. The resulting photocurrents, $i_1(t)$ and $i_2(t)$, are then processed to yield the average count rate on each

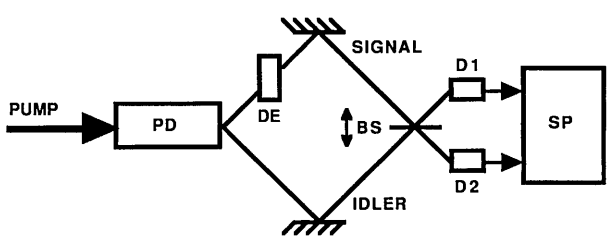

Fig. 1. Schematic for the dispersion-cancellation experiment of Steinberg *et al.*[13,14] PD, degenerate parametric downconverter; DE, dispersive element; BS, 50/50 beam splitter whose position is changed to vary the delay between the reflected signal and the idler beams reaching detectors D1 and D2, respectively; SP, signal processor used to measure the singles- and the coincidence-counting rates.

detector and the average coincidence-count rate. The singles rates can be found by calculation of

$$S_j(T) \equiv \langle i_j(t)\rangle/q \qquad \text{for } j = 1,2. \tag{50}$$

Because we are presuming operation in the low-photon-flux regime, the coincidence rate can be taken to be

$$C(T;\tau_g) \equiv q^{-2}\int \mathrm{d}\tau \langle i_1(t+\tau) i_2(t)\rangle \exp(-\tau^2/{\tau_g}^2), \tag{51}$$

where we have used a Gaussian window of duration τ_g to represent the gate within which counts must occur on both detectors to constitute a coincidence. Strictly speaking, we should include a pulse discriminator in our coincidence analysis. This is unnecessary if $P\tau_g \ll 1$. Under this condition there will be, with overwhelming probability, at most one signal–idler photon pair per gate interval. In the low-photon-flux regime it is not hard to meet the $P\tau_g \ll 1$ restriction while simultaneously satisfying the $\Delta\omega\tau_g \gg 1$ condition needed to produce dispersion cancellation; see below. These two conditions cannot be simultaneously enforced, however, in the high-photon-flux regime. When we study the Mach–Zehnder interferometer of Shih *et al.* we allow operation in the high-photon-flux regime without adding a pulse discriminator to our theory. This will correspond to performing intensity interferometry rather than photon-coincidence counting.

Before delving into the quantum calculations of $S_j(T)$ and $C(T;\tau_g)$, let us establish the semiclassical framework for finding these rates. The classical-field descriptions for the Fig. 1 experiment closely parallel the quantum formulation just given. In particular, the classical signal field emerging from the dispersive element, $E_{\mathrm{SD}}(t)$, is related to the classical field $E_S(t)$ that enters this element by Eq. (39) with the operator carets deleted. Just as in the quantum case, this linear filtering does not disturb the zero-mean-field, jointly Gaussian nature of the classical signal and idler beams. Furthermore, the correlation functions that are needed to characterize the joint statistics of $E_{\mathrm{SD}}(t)$ and $E_I(t)$ fully are easily shown to be

$$\langle {E_j}^*(t+\tau)E_k(t)\rangle = \delta_{jk}\exp(i\omega_j\tau)\int \frac{\mathrm{d}\omega}{2\pi}\,\mathcal{P}(\omega)\exp(i\omega\tau), \tag{52}$$

$$\langle E_j(t+\tau)E_k(t)\rangle = (1-\delta_{jk})\exp[-i(\omega_P t + \omega_j\tau)] \times \int \frac{\mathrm{d}\omega}{2\pi}\,\mathcal{P}(\omega)H(\omega)\exp(-i\omega\tau), \tag{53}$$

for $j = \mathrm{SD},I$ and $k = \mathrm{SD},I$. Applying the degeneracy condition and using the Gaussian spectrum from Eq. (9) specializes these equations to the following nonzero correlations:

$$\langle {E_{\mathrm{SD}}}^*(t+\tau)E_{\mathrm{SD}}(t)\rangle = \langle {E_I}^*(t+\tau)E_I(t)\rangle = P\exp(i\omega_P\tau/2 - \tau^2\Delta\omega^2/2), \tag{54}$$

$$\langle E_{\mathrm{SD}}(t+\tau)E_I(t)\rangle = \langle E_I(t+\tau)E_{\mathrm{SD}}(t)\rangle = \frac{P}{(1-i\ddot{\phi}\Delta\omega^2)^{1/2}} \times \exp\left[-i\omega_P(t+\tau/2) - \frac{\tau^2\Delta\omega^2/2}{1-i\ddot{\phi}\Delta\omega^2}\right]. \tag{55}$$

The beam-splitter relations, for the classical fields, are merely the quantum expressions, Eqs. (48) and (49), with the carets suppressed. The singles and the coincidence rates are calculated from the classical fields by means of the same photocurrent averages cited above, but now we must employ semiclassical-photodetection theory.

The quantum and the semiclassical models just established for the Fig. 1 experiment both predict identical, featureless singles rates for the two detectors,

$$S_j(T) = P \qquad \text{for } j = 1,2, \tag{56}$$

in both theories. In other words, there is no second-order interference in this setup. The coincidence rate is appreciably more complicated and more interesting.

Using the moment-factoring methods laid out in our photon-twins analysis, we have that $C(T;\tau_g)$ obeys Eq. (51) with

$$q^{-2}\langle i_1(t+\tau)i_2(t)\rangle = P^2 + 4^{-1}|\langle \hat{E}_{\mathrm{SD}}(t+\tau-T/2)\hat{E}_I(t+T/2)\rangle - \langle \hat{E}_I(t+\tau)\hat{E}_{\mathrm{SD}}(t)\rangle|^2 \tag{57}$$

in the quantum theory and

$$q^{-2}\langle i_1(t+\tau)i_2(t)\rangle = P^2 + 4^{-1}|\langle E_{\mathrm{SD}}(t+\tau-T/2)E_I(t+T/2)\rangle - \langle E_I(t+\tau)E_{\mathrm{SD}}(t)\rangle|^2 \tag{58}$$

in the semiclassical treatment.

Instead of presenting the most general forms of the resulting equations, we content ourselves with a particularly important special case. Specifically, we assume that the coincidence-gate duration τ_g is much longer than beam splitter's time delay T and also much longer than the dispersion-broadened signal–idler correlation time. Parametric downconverters have emission bandwidths of the order of 10^{13} s^{-1}, and practical coincidence gates are typically of the order of 1 ns; thus, even with a 20-fold dispersion of the signal–idler correlation, we are well within the regime of interest for the Fig. 1 configuration.[13] Consider first the quantum case. Without using the conditions just placed on τ_g, we have that

$$C(T;\tau_g) = P^2\sqrt{\pi}\,\tau_g + 4^{-1}\int \mathrm{d}\tau \frac{\sqrt{2}\,P\Delta\omega}{[\pi(1+4\ddot{\phi}^2\Delta\omega^4)]^{1/2}} \times \exp(-\tau^2/{\tau_g}^2)\left(\exp\left[-\frac{2(\tau-T)^2\Delta\omega^2}{1+4\ddot{\phi}^2\Delta\omega^4}\right] + \exp\left(-\frac{2\tau^2\Delta\omega^2}{1+4\ddot{\phi}^2\Delta\omega^4}\right) - 2\,\mathrm{Re}\left\{\exp\left[-\frac{(\tau-T)^2\Delta\omega^2}{1-2i\ddot{\phi}\Delta\omega^2}\right] \times \exp\left(-\frac{\tau^2\Delta\omega^2}{1+2i\ddot{\phi}\Delta\omega^2}\right)\right\}\right). \tag{59}$$

Now, assuming that $\tau_g \gg T$ and $\tau_g \gg (1+4\ddot{\phi}^2\Delta\omega^4)^{1/2}/\Delta\omega$ prevail, as stated just above, we can delete the $\exp(-\tau^2/{\tau_g}^2)$ factor from the integral in Eq. (59). What remains can be integrated in closed

form, with the following result:

$$C(T;\tau_g) = P\{\sqrt{\pi}\,P\tau_g + 2^{-1}[1-\exp(-\Delta\omega^2 T^2/2)]\}. \quad (60)$$

A similar calculation for the semiclassical theory implies

$$C(T;\tau_g) = \sqrt{\pi}\,P^2\tau_g\{1+(2\Delta\omega\tau_g)^{-1}[1-\exp(-\Delta\omega^2 T^2/4)]\}. \quad (61)$$

Both of these expressions apply for all values of the dispersion constant $\ddot{\phi}$; hence both show complete dispersion cancellation in the transform-limited widths of their minima at $T = 0$. Note that there is nothing intrinsically quantum mechanical about the dispersion cancellation in the Fig. 1 arrangement. Its origin is easily traced to the fact that the four correlation functions appearing in Eqs. (57) and (58) are dispersion-broadened, chirped-Gaussian functions. The negative contributions to Eqs. (60) and (61) derive from cross terms created by the magnitude-squaring operation in Eqs. (57) and (58); see, e.g., the Re{} term in the integrand of Eq. (59). When these cross terms are integrated over the τ_g-s gate interval, they behave like the matched-filter pulse compressors found in chirped-pulse radar systems.[29]

The term $\sqrt{\pi}\,P^2\tau_g$ in the quantum formula, Eq. (60), represents accidental coincidences, which occur when each detector registers a count within a common gate interval but when the detected photons are not an entangled signal–idler pair. For the low photon fluxes that are prototypical of parametric downconversion, nanosecond gate durations will give $P\tau_g \ll 1$; hence the $T = 0$ coincidence-rate dip constitutes an essentially 100%-visibility white-light fringe. That is, we have that[30]

$$\gamma \equiv \frac{\max_T[C(T;\tau_g)] - \min_T[C(T;\tau_g)]}{\max_T[C(T;\tau_g)] + \min_T[C(T;\tau_g)]} \quad (62)$$

$$= 1/(1+4\sqrt{\pi}\,P\tau_g) \approx 1 \qquad \text{for } P\tau_g \ll 1. \quad (63)$$

The same $\sqrt{\pi}\,P^2\tau_g$ term appears on the right-hand side in the semiclassical expression, Eq. (61), where its effect is far more pronounced. Indeed, in the semiclassical case it completely masks the white-light fringe at $T = 0$. Because dispersion cancellation requires that $\Delta\omega\tau_g \gg 1$, Eq. (61) implies that γ is, from Eq. (62),

$$\gamma = 1/(1+4\Delta\omega\tau_g) \ll 1 \qquad \text{for } \Delta\omega\tau_g \gg 1. \quad (64)$$

Thus, a dispersion-cancellation experiment of the Fig. 1 variety that is performed on Gaussian-state light in the low-photon-flux regime can be said to show a nonclassical effect even with fringe visibilities substantially less than 50%.

Restricting our semiclassical versus quantum fringe-visibility comparison to Gaussian-state light is quite reasonable. After all, as is shown in Section 2, this restriction includes the only classical-field model that reproduces all the signal-only and idler-only photodetection statistics of the quantum model. Nevertheless, before turning to the Mach–Zehnder interferometer of Shih *et al.*, let us address the nonergodic classical-field model that previous studies have asserted yields 50% fourth-order fringe visibility.

In lieu of the classical-field model from Subsection 2.B, we now assume that $E_S(t)$ and $E_I(t)$ are classically random, positive-frequency, photon-units signal and idler fields obeying

$$E_S(t) = \sqrt{P}\exp[-i(\omega_S+\tilde{\omega})t - i\tilde{\theta}], \quad (65)$$

$$E_I(t) = \sqrt{P}\exp[-i(\omega_I-\tilde{\omega})t + i\tilde{\theta}], \quad (66)$$

where $\tilde{\omega}$ and $\tilde{\theta}$ are statistically independent random variables, with the former being Gaussian with mean zero and variance $\Delta\omega^2$ and the latter being uniformly distributed on $[0, 2\pi]$. This model is not ergodic,[31,32] but if $\tilde{\omega}$ and $\tilde{\theta}$ are made slowly varying functions of time then we can still use the ensemble-average analysis based on Eqs. (65) and (66) as representative of a real, time-averaged measurement.

Equations (65) and (66) have the same ensemble-average mean functions and correlation functions as the Gaussian model from Subsection 2.B. Thus, when this nonergodic classical-field model is used to analyze the dispersion-cancellation experiment, it reproduces the semiclassical singles-rate prediction given above. On the other hand, Eqs. (65) and (66) no longer permit the use of the Gaussian moment-factoring theorem. So their application to modeling the dispersion-cancellation experiment's coincidence rate requires a new calculation. Thankfully, this calculation is simple. Because $E_S(t)$ is monochromatic, we have that

$$E_{SD}(t) = \sqrt{P}\,H(\tilde{\omega})\exp[-i(\omega_S+\tilde{\omega})t - i\tilde{\theta}]. \quad (67)$$

The photocurrent cross-correlation function needed for evaluation of Eq. (51) is then found to be

$$q^{-2}\langle i_1(t+\tau)i_2(t)\rangle = \langle |E_1(t+\tau)|^2|E_2(t)|^2\rangle \quad (68)$$

$$= P^2(1-2^{-1}\,\mathrm{Re}\{\langle\exp[i\tilde{\omega}(2\tau - T)]\rangle\}) \quad (69)$$

$$= P^2\{1-2^{-1}\exp[-2(\tau-T/2)^2\Delta\omega^2]\}. \quad (70)$$

Clearly there is a transform-limited, 50% fringe-visibility feature in this cross-correlation function at $\tau = T/2$. However, to evaluate the coincidence rate we must substitute Eq. (70) into Eq. (51) and integrate. Continuing our assumption that $\Delta\omega\tau_g \gg 1$ holds, this integration yields

$$C(T;\tau_g) = P^2\sqrt{\pi}\,\tau_g[1-(\sqrt{8}\,\Delta\omega\tau_g)^{-1}\exp(-T^2/4\tau_g^2)]. \quad (71)$$

This result is very different from the low-photon-flux quantum behavior exhibited in Eq. (60). First, the peak coincidence rate is proportional to P^2, not to P. Second, the dip at $T = 0$ is coincidence-gate limited, not transform limited. Finally, the fringe visibility is much smaller than 50%. Indeed, the nonergodic model's fringe visibility is similar to that found earlier for our Gaussian-state classical-field model. In this regard we note that Franson[33] previously refuted the claim that Eqs. (65) and (66) yield high-visibility fourth-order interference fringes. Also, Ou and Mandel[32] showed that ergodic classical-field models have a maximum fourth-order interference fringe visibility of approximately (in our notation) $1/\Delta\omega\tau_g$.[34] Taken collectively, these results make it clear that purely quantum effects can be claimed in fourth-order interference at fringe visibilities far below 50%.

B. Mach–Zehnder Interferometer

Figure 2 shows a schematic of the fourth-order interference experiment of Shih *et al.*[15] Signal and idler beams are obtained from a nondegenerate parametric downconverter and applied to one input port of a Mach–Zehnder interferometer. One output beam from the interferometer is transmitted through an optical passband filter for the signal beam, and the other is sent to an optical passband filter that transmits the idler beam. These optically filtered outputs illuminate two photodetectors, from which time-averaged single-detector-count rates and a coincidence-count rate are determined as functions of T, the time delay between the two arms of the interferometer.

The analysis of this arrangement, using our quantum and semiclassical theories, overlaps heavily with our treatment of dispersion cancellation. Basically, the main thing that needs to be done is to relate the fields illuminating the photodetectors to the signal and the idler beams produced by the downconverter. By means of the nondegeneracy condition, $|\omega_S - \omega_I| \gg \Delta\omega$, we can assume ideal optical filters and say that

$$E_S^{\text{out}}(t) \equiv [E_S(t - T) + E_S(t)]/2, \tag{72}$$

$$E_I^{\text{out}}(t) \equiv [E_I(t) - E_I(t - T)]/2 \tag{73}$$

are the classical fields that illuminate detectors DS and DI—the signal-beam and idler-beam detectors, respectively—in a semiclassical analysis of Fig. 2. Strictly speaking, merely adding operator carets to Eqs. (72) and (73) will not suffice for the quantum theory; the vacuum-field contributions entering through the unused input port in Fig. 2 must be explicitly accounted for to properly preserve the commutator brackets.[11] These vacuum-state fields will not affect our calculations, however. This is because the quantum signal and idler fields emerging from the passband filters commute with each other and with each other's adjoint. Thus we can perform the quantum coincidence-rate calculation by using normally ordered fourth moments without encountering any nonzero commutators, and we can find these moments correctly merely by placing operator carets on all the fields in Eqs. (72) and (73).

With the Gaussian-spectrum field models from Section 2, both quantum and semiclassical photodetection give the identical, second-order interference results for the singles rates, that is,

$$S_j(T) = \langle i_j(t)\rangle/q = \begin{cases} (P/2)[1 + \exp(-\Delta\omega^2 T^2/2)\cos(\omega_S T)] & \text{for } j = S \\ (P/2)[1 - \exp(-\Delta\omega^2 T^2/2)\cos(\omega_I T)] & \text{for } j = I \end{cases}, \tag{74}$$

where $i_S(t)$ and $i_I(t)$ are the photocurrents from the signal and the idler detectors in Fig. 2. Sensed individually, the signal and the idler beams show fringes at their respective center frequencies with a visibility that decreases from unity at $T = 0$ to essentially nil when $\Delta\omega T \gg 1$. Given our comments at the conclusion of Subsection 2.B, this congruence of the singles rates predicted by our two models is to be expected.

The coincidence rate for the Fig. 2 setup is found, in either photodetection theory, from

$$C(T; \tau_g) = q^{-2} \int d\tau \langle i_S(t + \tau) i_I(t)\rangle \exp(-\tau^2/\tau_g^2), \tag{75}$$

where once again we use a τ_g-s Gaussian coincidence window and omit a pulse discriminator. Shih *et al.* developed the low-photon-flux quantum theory for a quantity similar to $C(T; \tau_g)$, using the correlated single-photon wave packet method, in the study reported in Ref. 35. They identify and study three physically interesting cases, which, in our notation, are as follows.

Short Delay: $\tau_g \gg \Delta\omega^{-1} \gg T$. Perfect second-order fringes are formed in the singles measurements, and the coincidence rate has fringes in T at frequencies ω_S, ω_I, ω_P, and $\omega_S - \omega_I$.

Medium Delay: $\tau_g \gg T \gg \Delta\omega^{-1}$. There is no second-order interference, and the coincidence rate has fringes in T only at frequency ω_P with 50% fringe visibility.

Long Delay: $T \gg \tau_g \gg \Delta\omega^{-1}$. Again there is no second-order interference, and the coincidence rate has fringes in T only at frequency ω_P, but with 100% visibility.

Our Gaussian field-correlation approach to the quantum theory will reproduce all three of the low-photon-flux photon-coincidence cases of Shih *et al.* In addition, it handles the same delay cases for high-photon-flux intensity interferometry. Furthermore, because we have an accompanying semiclassical theory, our technique re-

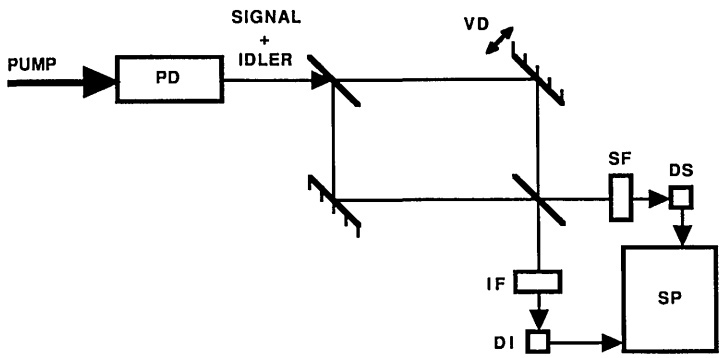

Fig. 2. Schematic for the fourth-order interference Mach–Zehnder interferometer of Shih *et al.*[15] PD, nondegenerate parametric downconverter; VD, variable delay between the interferometer's two arms; SF and IF, respectively, the signal-beam and the idler-beam passband optical filters; DS and DI, respectively, the signal-beam and the idler-beam detectors; SP, signal processor used to measure the singles- and the coincidence-counting rates.

veals the conditions under which a purely quantum effect can be claimed in either the low-photon-flux or the high-photon-flux limit.[36]

The route to obtaining quantum and semiclassical formulas for $C(T;\tau_g)$ is, by now, a familiar one: find the photocurrent cross correlation needed for evaluation of Eq. (75) by successive use of the interferometer's field transformation, the Gaussian moment-factoring theorem, and the spectrum from Eq. (9). In the quantum theory this gives

$$q^{-2}\langle i_S(t+\tau)i_I(t)\rangle = S_S(T)S_I(T) + (1/16)|\langle[\hat{E}_S(t+\tau-T)+\hat{E}_S(t+\tau)] \times [\hat{E}_I(t)-\hat{E}_I(t-T)]\rangle|^2, \quad (76)$$

which we are to evaluate by using Eq. (74) for the singles rates $\{S_j(T)\}$ and, for the rest of the equation, by multiplying out and averaging term by term inside the brackets, using Eqs. (3) and (9). In the semiclassical theory the corresponding result is

$$q^{-2}\langle i_S(t+\tau)i_I(t)\rangle = S_S(T)S_I(T) + (1/16)|\langle[E_S(t+\tau-T)+E_S(t+\tau)] \times [E_I(t)-E_I(t-T)]\rangle|^2, \quad (77)$$

which for the singles rate we are to evaluate by using Eq. (74) and for the rest of the equation by multiplying out inside the averaging brackets and then substituting Eq. (17) for the signal–idler correlation. Both Eqs. (76) and (77) lead to the same fringe taxonomy cited above.

Short Delay: $\tau_g \gg \Delta\omega^{-1} \gg T$,

$$C(T;\tau_g) = 4^{-1}(\sqrt{\pi}P^2\tau_g + K)\{1+\cos(\omega_S T)-\cos(\omega_I T) - 2^{-1}\cos[(\omega_S-\omega_I)T]-2^{-1}\cos(\omega_P T)\}. \quad (78)$$

Medium Delay: $\tau_g \gg T \gg \Delta\omega^{-1}$,

$$C(T;\tau_g) = 4^{-1}\{\sqrt{\pi}P^2\tau_g + K[1-2^{-1}\cos(\omega_P T)]\}. \quad (79)$$

Long Delay: $T \gg \tau_g \gg \Delta\omega^{-1}$,

$$C(T;\tau_g) = 4^{-1}\{\sqrt{\pi}P^2\tau_g + (K/2)[1-\cos(\omega_P T)]\}. \quad (80)$$

Equations (78)–(80) apply for all values of $P/\Delta\omega$, i.e., in both the low-photon-flux and the high-photon-flux regimes. In these expressions the constant K is given by

$$K = \int \frac{d\omega}{2\pi}\,\mathcal{P}(\omega)[\mathcal{P}(\omega)+1] = \sqrt{\pi}P^2/\Delta\omega + P \quad (81)$$

in the quantum theory and by

$$K = \int \frac{d\omega}{2\pi}\,\mathcal{P}^2(\omega) = \sqrt{\pi}P^2/\Delta\omega \quad (82)$$

in the semiclassical theory. Evidently the fringe taxonomy of the Mach–Zehnder interferometer is derived entirely from its classical field-propagation equations; only the constant K distinguishes the quantum and the semiclassical theories. Moreover, it should come as no surprise that the quantum and the semiclassical K formulas differ precisely by the appearance, in the former, of the much-discussed +1 term from Section 2. Our final task will be to determine the minimum fringe visibility beyond which observation of a purely quantum effect can be asserted. Only the long-delay case will be treated; the others can be handled in similar, straightforward manners.

When we operate in the long-delay region, the coincidence rate has a time-delay fringe at the pump frequency ω_P; the fringe's visibility is, from Eq. (62) and Eqs. (80)–(82),

$$\gamma = \begin{cases} \dfrac{1+(\Delta\omega/\sqrt{\pi}P)}{1+2\Delta\omega\tau_g+(\Delta\omega/\sqrt{\pi}P)} & \text{quantum mechanically} \\ \dfrac{1}{1+2\Delta\omega\tau_g} & \text{semiclassically} \end{cases}. \quad (83)$$

In the low-photon-flux regime we have that $P/\Delta\omega \ll 1$, and we can simultaneously keep τ_g small enough to ensure that $P\tau_g \ll 1$. When these conditions are imposed on Eq. (83), we get

$$\gamma \approx \begin{cases} 1 & \text{quantum mechanically} \\ 1/2\Delta\omega\tau_g \ll 1 & \text{semiclassically} \end{cases}, \quad (84)$$

where the last inequality is due to $\tau_g \gg \Delta\omega^{-1}$. Thus the quantum theory predicts near-unity visibility, whereas the semiclassical theory argues for very weak fringes. Because our semiclassical model employs classical fields of maximum signal–idler correlation, the semiclassical portion of Eq. (84) represents the threshold for claiming a purely quantum effect.[36] As in our study of the dispersion-cancellation experiment, we see that fourth-order interference in a low-photon-flux Mach–Zehnder interferometer is nonclassical at fringe visibilities well below unity.

For intensity interferometry in the high-photon-flux regime, wherein $P/\Delta\omega \gg 1$ holds, we find that the semiclassical fringe visibility is unchanged from its low-photon-flux values but that there is a dramatic reduction in the quantum fringe visibility. Using γ_{SC} to denote the semiclassical member of Eq. (83), we have that

$$\gamma_Q \approx \gamma_{SC} + 1/2\sqrt{\pi}P\tau_g \ll 1 \quad (85)$$

is the high-photon-flux quantum fringe visibility in the long-delay case. So there is still a nonclassical fringe visibility in high-photon-flux intensity interferometry, but it is a weak effect:

$$\gamma_Q/\gamma_{SC} \approx 1 + \Delta\omega/\sqrt{\pi}P \approx 1 \quad (86)$$

for this measurement.

4. CONCLUSIONS

We have used the Gaussian field-correlation approach to provide unified quantum and semiclassical theories for squeezing, photon twins, and fourth-order interference measurements made on the signal and the idler beams

from a parametric downconverter. All three measurements exhibit purely quantum signatures arising from the nonclassical behavior of the phase-sensitive correlation between the signal and the idler beams. Whereas previous research used field correlations to study squeezing and photon twins, we believe that our investigation provides the first such treatment for fourth-order interference. As such, it shows that nonclassical effects can be said to occur, at low photon fluxes, with observed fourth-order fringe visibilities well below unity. In addition it establishes a distinction between the classical nature of linear field filtering, such as that underlying dispersion cancellation, and its nonclassical observation through fourth-order interference, which relies on the entangled signal–idler state produced by a parametric downconverter. Furthermore, our formalism offers the following qualitative comparison of these three nonclassical $\chi^{(2)}$ effects.

Quadrature Noise Squeezing: Equation (24) embodies the nonclassical signature of squeezing. Strong squeezing is seen only as the high-photon-flux limit is approached. Moreover, the resulting nonclassical behavior is degraded by subunity detector quantum efficiency, i.e., Eq. (24) becomes

$$S_{\min}(\omega) = \begin{cases} q^2\eta P_{\mathrm{LO}}((1-\eta)+\eta\{[1+\mathcal{P}(\omega)]^{1/2}-[\mathcal{P}(\omega)]^{1/2}\}^2) & \text{quantum theory} \\ q^2\eta P_{\mathrm{LO}} & \text{semiclassical theory} \end{cases}, \quad (87)$$

when detectors of quantum efficiency η are used. Thus, cw quadrature-noise squeezing is best demonstrated in resonant-cavity $\chi^{(2)}$ systems, where $\mathcal{P}(\omega) \sim 1$ can be reached at radio-frequency ω with high-quantum-efficiency homodyne receivers.

Photon Twins: Equations (37) and (38) characterize the semiclassical and the quantum variances of the per-unit-time photocount difference. Unlike in the situation for squeezing, the strength of the nonclassical photon-twin signature implied by these formulas is independent of whether operation is in the low-photon-flux regime. Once again, high-quantum-efficiency detection is necessary, i.e., Eqs. (37) and (38) change to

$$\langle \Delta N_T{}^2\rangle/T = 2\eta P \qquad \text{for all } T, \quad (88)$$

$$\langle \Delta N_T{}^2\rangle/T \to \begin{cases} 2\eta P & \text{as } \Delta\omega T \to 0 \\ 2\eta(1-\eta)P & \text{as } \Delta\omega T \to \infty \end{cases}, \quad (89)$$

respectively, when detectors of quantum efficiency η are used.

Fourth-Order Interference: Equation (83) contrasts the quantum and the semiclassical fringe visibilities in a particular, but nonetheless representative, fourth-order interference experiment. Here a strong nonclassical signature is available only in the low-photon-flux regime. Unlike in the situations for squeezing and photon twins, however, the nonclassical signature of fourth-order interference is independent of the detector quantum efficiency, i.e., Eq. (83) applies even if detectors of quantum efficiency $\eta < 1$ are employed.

*Present address, Edward Ginzton Laboratory, Stanford University, Stanford, California 94305-4085.

REFERENCES AND NOTES

1. L.-A. Wu, H. J. Kimble, J. L. Hall, and H. Wu, "Generation of squeezed states by parametric downconversion," Phys. Rev. Lett. **57,** 2520 (1986).
2. A. Heidmann, R. J. Horowicz, S. Reynaud, E. Giacobino, C. Fabre, and G. Camy, "Observation of quantum noise reduction on twin laser beams," Phys. Rev. Lett. **59,** 2555 (1987).
3. A. Aspect, P. Grangier, and G. Roger, "Dualité onde-particule pour un photon unique," J. Opt. (Paris) **20,** 119 (1989).
4. R. Ghosh and L. Mandel, "Observation of nonclassical effects in the interference of two photons," Phys. Rev. Lett. **59,** 1903 (1987).
5. L.-A. Wu, M. Xiao, and H. J. Kimble, "Squeezed states of light from an optical parametric oscillator," J. Opt. Soc. Am. B **4,** 1465 (1987).
6. S. Reynaud, C. Fabre, and E. Giacobino, "Quantum fluctuations in a two-mode parametric oscillator," J. Opt. Soc. Am. B **4,** 1520 (1987).
7. N. C. Wong, K. W. Leong, and J. H. Shapiro, "Quantum correlation and absorption spectroscopy in an optical parametric oscillator in the presence of pump noise," Opt. Lett. **15,** 891 (1990).
8. R. Ghosh, C. K. Hong, Z. Y. Ou, and L. Mandel, "Interference of two photons in parametric downconversion," Phys. Rev. A **34,** 3962 (1986).
9. R. A. Campos, B. E. A. Saleh, and M. C. Teich, "Fourth-order interference of joint single-photon wave packets in lossless optical systems," Phys. Rev. A **42,** 4127 (1990).
10. H. P. Yuen and J. H. Shapiro, "Optical communication with two-photon coherent states—Part III: Quantum measurements realizable with photoemissive detectors," IEEE Trans. Inf. Theory **IT-26,** 78 (1980).
11. C. M. Caves, "Quantum-mechanical noise in an interferometer," Phys. Rev. D **23,** 1693 (1981).
12. M. H. Rubin and Y. H. Shih, "Models of a two-photon Einstein–Podolsky–Rosen interference experiment," Phys. Rev. A **45,** 8138 (1992).
13. A. M. Steinberg, P. G. Kwiat, and R. Y. Chiao, "Dispersion cancellation in a measurement of the single-photon propagation velocity," Phys. Rev. Lett. **68,** 2421 (1992).
14. A. M. Steinberg, P. G. Kwiat, and R. Y. Chiao, "Dispersion cancellation and high-resolution time measurements in a fourth-order optical interferometer," Phys. Rev. A **45,** 6659 (1992).
15. Y. H. Shih, A. V. Sergienko, T. E. Kiess, M. H. Rubin, and C. O. Alley, "Two-photon interference in a standard Mach–Zehnder interferometer," in *Quantum Electronics and Laser Science Conference*, Vol. 12 of 1993 OSA Technical Digest Series (Optical Society of America, Washington, D.C., 1993), p. 273.
16. J. H. Shapiro, "Quantum noise and excess noise in optical homodyne and heterodyne receivers," IEEE J. Quantum Electron. **QE-21,** 237 (1985).
17. Because we have suppressed the spatial and polarization characteristics of these fields, we say that our parametric interaction is degenerate if $\omega_S = \omega_I = \omega_P/2$ and nondegenerate if $|\omega_S - \omega_I| \gg \Delta\omega$, where $\Delta\omega$ is the common bandwidth of the signal and the idler emissions. Our development implicitly assumes that the signal and the idler beams are nondegenerate in either space or in polarization when they are degenerate in frequency. Spatial nondegeneracy is ordinarily the case in parametric downconverters, and type-II phase-matched OPA's and OPO's produce orthogonally polarized signal and idler beams, so little generality is lost through this implicit assumption.
18. L. G. Joneckis and J. H. Shapiro, "Quantum propagation in a Kerr medium: lossless dispersionless fiber," J. Opt. Soc. Am. B **10,** 1102 (1993).
19. H. P. Yuen, "Two-photon coherent states of the radiation field," Phys. Rev. A **13,** 2226 (1976).
20. Because well-known procedures are available for accounting for subunity quantum efficiency in both quantum and semiclassical photodetection (see, e.g., Ref. 16), we treat only the ideal case of unity quantum efficiency. Furthermore, because our principal goal is to study the semiclassical and quantum fringe visibilities in fourth-order interference ex-

periments, it is worth noting that these visibilities are independent of detector quantum efficiency; see the quantum efficiency discussion in Section 4.
21. J. H. Shapiro, G. Saplakoglu, S.-T. Ho, P. Kumar, B. E. A. Saleh, and M. C. Teich, "Theory of light detection in the presence of feedback," J. Opt. Soc. Am. B **4,** 1604 (1987).
22. In deriving Eqs. (22) and (23), we use our assumption that $\mathcal{P}(\omega)$ is an even function. If this assumption is relaxed, then Eqs. (22) and (23) should be replaced by the even parts of the expressions shown in the text. This change does not affect the essential conclusion: the semiclassical noise level always equals or exceeds the shot-noise level, whereas the quantum theory can have noise lower than the shot-noise limit.
23. It is well known that fourth moments of zero-mean, jointly Gaussian random variables factor into sums of products of their second moments; see, e.g., Ref. 24. For an arbitrary Gaussian state this classical result can be combined with the quantum theory of heterodyne detection[10] to produce a quantum moment-factoring theorem for antinormally ordered field-operator moments. The normally ordered fourth-moment result that we employ is then found by repeated use of the delta-function commutator.
24. J. M. Wozencraft and I. M. Jacobs, *Principles of Communication Engineering* (Wiley, New York, 1965), p. 205.
25. This result does not depend on assuming that $\mathcal{P}(\omega)$ is an even function.
26. C. K. Hong, Z. Y. Ou, and L. Mandel, "Measurement of subpicosecond time intervals between two photons by interference," Phys. Rev. Lett. **59,** 2044 (1987).
27. This quantum preservation of joint Gaussian behavior is just like the well-known result for classical Gaussian random processes (see, e.g., Ref. 24, Chap. 3). It can be proved by performance of the state transformation implied by Eq. (39) with antinormally ordered characteristic functions.[28]
28. H. P. Yuen and J. H. Shapiro, "Optical communication with two-photon coherent states—Part I: Quantum state propagation and quantum-noise reduction," IEEE Transf. Inf. Theory **IT-24,** 657 (1978).
29. M. I. Skolnik, *Introduction to Radar Systems* (McGraw-Hill, New York, 1980) Chap. 11.
30. Strictly speaking, we are concerned with a coincidence-rate dip at $T = 0$, not with a white-light fringe. Thus an experimentalist might prefer to gauge the depth of the destructive interference that occurs at $T = 0$ by computing $\{\max_T[C(T; \tau_g)] - \min_T[C(T; \tau_g)]\}/\max_T[C(T; \tau_g)]$ rather than γ.
31. Z. Y. Ou, X. Y. Zou, L. J. Wang, and L. Mandel, "Observation of nonlocal interference in separated photon channels," Phys. Rev. Lett. **65,** 321 (1990).
32. Z. Y. Ou and L. Mandel, "Classical treatment of the Franson two-photon correlation experiment," J. Opt. Soc. Am. B **7,** 2127 (1990).
33. J. D. Franson, "Violation of a simple inequality for classical fields," Phys. Rev. Lett. **67,** 290 (1991).
34. The configuration considered by Ou and Mandel[32] is not that of the dispersion-cancellation experiment. Their principal assumption, however, is configuration independent; they require the coincidence-gate duration to be much longer than both the field- and the intensity-correlation times of the signal and the idler beams. Thus the Ou–Mandel proof can be adapted to the Fig. 1 configuration.
35. Y. H. Shih, A. V. Sergienko, M. H. Rubin, T. E. Kiess, and C. O. Alley, "Two-photon interference in a standard Mach–Zehnder interferometer," Phys. Rev. A (to be published).
36. Our concluding analysis from Subsection 3.A can be adapted to show that the nonergodic classical-field model from Eqs. (65) and (66) does not predict high-visibility coincidence-rate fringes. The Ou–Mandel theory[32] can be used to disqualify any ergodic model from producing high-visibility fringes.